Polymer Degradation and Stability 94 (2009) 1814–1824

Contents lists available at ScienceDirect

Polymer Degradation and Stability

journal homepage: www.elsevier.com/locate/polydegstab

An investigation of the accelerated thermal degradation of different epoxy resin composites using X-ray microcomputed tomography and optical coherence tomography

Firas Awaja [a,*], Benedicta Arhatari [b], Karin Wiesauer [c], Elisabeth Leiss [c], David Stifter [d]

[a] Centre for Material and Fibre Innovation, Geelong Technology Precinct, Deakin University, Geelong, Victoria 3217, Australia
[b] Department of Physics, La Trobe University, Victoria 3086, Australia
[c] Recendt GmbH, Hafenstrasse 47-51, 4020 Linz, Austria
[d] Center for Surface and Nanoanalytics – ZONA, Johannes Kepler University Linz, Altenbergerstrasse 69, 4040 Linz, Austria

ARTICLE INFO

Article history:
Received 22 April 2009
Received in revised form
16 May 2009
Accepted 8 June 2009
Available online 17 June 2009

Keywords:
Syntactic foam
X-ray computed tomography
Epoxy resin
Optical coherence tomography
Thermal damage

ABSTRACT

Epoxy resin composites reinforced with hollow glass microspheres, microlight microspheres, 3D parabeam glass, and E-Glass individually were subjected to accelerated thermal degradation conditions. X-ray microcomputed tomography (XμCT) was used to evaluate density changes, reinforcement filler damage, homogeneity, cracks and microcracks in the bulk of the different epoxy resin composites. XμCT 3D images, 2D reconstructed images and voids calculations revealed microspheres damage, filler distributions and showed cracks in all composites with different shapes and volume in response to the thermal degradation conditions. In addition, expansion of air bubbles/voids was observed and recorded in the microsphere and microlight epoxy composite samples. In a complementary way, optical coherence tomography (OCT) was used as a novel optical characterisation technique to study structural changes of the surface and near-surface regions of the composites, uncovering signs of surface shrinkage caused by the thermal treatment. Thus, combining XμCT and OCT proved useful in examining epoxy resin composites' structure, filler–resin interface and surface characteristics.

1. Introduction

Polymer composites used in the automotive, marine, aerospace and space industries are required to perform in conditions where they may undergo severe mechanical, thermal and chemical damage. Replacing or repairing damaged parts is often expensive and difficult especially in the case of space and aerospace structures, aircraft and equipment. Syntactic foam-like resin filled with glass microsphere or microlight are used in many applications such as for buoyancy in marine environments, as a core material in sandwich structures used in aerospace and as thermal insulations of oil pipelines and structural components [1–3]. These materials have the advantage of a high specific strength to weight ratio. Glass and carbon fibre-reinforced epoxy resin composites are widely used in many applications due to its favourable mechanical properties [4–6]. These composites are expected to perform under harsh environmental conditions for a long period of time [5,6].

Polymer structural damage can be classified into macro and microscopic levels. The macroscopic damage often occurs as a result of an impact stress. Cracks, structural defects and delamination that are formed deep into the structure of polymer composites are extremely difficult to detect and to repair [7]. These internal defects not only decrease the material performance but also serve as catalysts for further damage like macrocracks [8], moisture swelling [7] and debonding [7]. Microscopic scale damage such as microcracks occurs as a result of impact and internal stresses. Microcracks are the major cause of material failure due to their nature of being undetected and also due to the induced structure fragmentation which leads to the reduction of mechanical properties such as strength, stiffness and dimensional stabilities [7,8]. Damage like microcracking is difficult to detect due to the resolution limit of the inspection technique and hence it cannot be repaired [8,9]. Epoxy resin composites failure commonly occurs as single layer breakdown such as the cracking of the fibre or the epoxy resin. Fibre elastic buckling and separation from the resin matrix were also reported as a typical composite failure [10,11].

* Corresponding author. Present address: School of Physics, University of Sydney, Sydney 2006, NSW, Australia.
E-mail address: firas@physics.usyd.edu.au (F. Awaja).

0141-3910/$ – see front matter © 2009 Elsevier Ltd. All rights reserved.
doi:10.1016/j.polymdegradstab.2009.06.005

Thermal stress generates mechanical pressure on the surface and the bulk of the matrix resulting in crack initiation and propagation. Surface oxidation at high temperature and energy results in an increase of surface density as a result of outgassing of volatiles and shrinkage which also leads to the generation of cracks [12–14]. Oxidative thermal stress cycles have been used previously in accelerated degradation studies of different resin systems [15–19]. Lafarie-Frenot et al. [16] showed that thermo-mechanical damage resulted stress cracks of their carbon-fibre/epoxy resin laminate. Decelle et al. [17] reported that shrinkage in the surface layer of the resin matrix and an increase in the density were observed as a result of the resin oxidation during ageing at 150 °C. The departure of volatiles from the surface and the oxygen diffusion into the bulk of the polymer led to an increase in surface densities and reduction in bulk mechanical properties which resulted in stress cracks [18,19].

X-ray microcomputed tomography (XμCT) is a structure visualization technology in the field of non-destructive testing. XμCT allows not only for the visualization of the volumetric nature of the sample microstructure but also for the use of the 3D image data to evaluate the sample quantitatively. X-ray tomography has been used previously in inspecting mechanically and thermally induced polymer composite damages [20–22]. Beier et al. [20] reported that resin rich and fibre defects were observed in a stitched NCF composite from the tomography images. Awaja and Arhatari [21] used XμCT to explain inner structure damage of syntactic foam under thermal cycle degradation conditions. They reported different types of filler damage and the role of expanding voids in the generation of cracks. Schilling et al. [22] reported internal damage, including delamination and microcracking, in mechanically damaged fibre-reinforced polymer–matrix composite materials utilising XμCT.

Optical coherence tomography (OCT) is a novel imaging method which was recently developed for applications in the area of biomedical diagnostics and which provides in a contactless and non-destructive way high-resolution cross-sectional images of the internal structure of turbid and scattering tissue and materials [23]. In contrast to XμCT, OCT operates in reflection geometry with harmless broadband light in the near-infrared spectral range illuminating the tissue/sample under investigation, enabling e.g. *in vivo* diagnostics of retinal diseases in ophthalmology. Beside the original OCT method, a multitude of instrumental extensions and modifications have been presented in recent years [24], involving developments like ultrahigh-resolution OCT (UHR-OCT) imaging with depth resolutions down to the micrometer range or the spectral-domain OCT (SD-OCT) technique with unprecedented imaging speed and sensitivity [25]. Also these extensions – like the original OCT method – are almost exclusively employed for applications in the field medical diagnostics. However, novel and alternative applications outside the biomedical field are gaining momentum, as summarized in a recent review [26] demonstrating that OCT can also be used for structural imaging in semi-transparent and scattering polymer and composite materials for e.g. defect detection and strain analysis.

This study aims at thoroughly inspecting the inner structure of different epoxy resin composites subjected to accelerated thermal degradation using XμCT. In a complementary way, OCT is used – to the best of our knowledge for the first time – to study the effect of the thermal treatment on the surface/near-surface region of the composites, thus essentially contributing to a more complete description of the occurring degradation process. In total, the XμCT and OCT investigations were designed to reveal information regarding epoxy resin composites density changes, reinforcement filler damage, homogeneity, cracks and microcracks, void expansion and surface shrinkage as a result of accelerated thermal degradation conditions.

2. Experimental

2.1. Materials

KINETIX R246TX epoxy resin (ATL Composites, Australia) was used in this study, consisting of diglycidyl ether of bisphenol A (DGEBA)/diglycidyl ether of bisphenol F (DGEBF) resin blend with an aliphatic glycidylether functional diluent. Super fast hardener, KINETIX H126 (ATL Composites, Australia), manufactured to cure at room temperature is an aliphatic/cycloaliphatic amine, with isophorone diamine being the main ingredient.

Hollow glass microspheres were used to produce syntactic foam for this study. The glass microsphere is West System blend 411 (Saint-Gobain RF Pty Ltd, Australia). It's a combination of inorganic hollow spheres and colloidal silica. It has an actual density of 0.18 g/cc and bulk density of 0.11 g/cc. The spheres size is varied between 5 and 200 μm in diameter. The XμCT 3D image of the hollow glass microspheres is shown in Fig. 1. Microlight microsphere filler (West System 410, Saint-Gobain Pty Ltd, Australia) is a lightweight fairing compound (Sp. Gr. = 0.1). It is mainly a blend of thermoplastic and sodium borosilicate microsphere. Fig. 2 shows the XμCT 3D image of the microlight filler microspheres. Figs. 1 and 2 were produced by 3D rendering from tomography data. The syntactic foam was made by adding the glass microsphere to the resin and mixing for 10 min. Then the hardener was added to the mixture, which was mixed for further 5 min and was laid up in Teflon mould. The resin to hardener ratio was 4:1 as recommended by the manufacturer. The microsphere percentage was 40% of the total volume. Same procedure was followed with the microlight microsphere composite using same mixing percentages. The initial curing was conducted according to the manufacturer recommendations and at room temperature (22 °C) while post-curing condition were set at 100 °C for 4 h.

Two other types of reinforcement were also selected for composite manufacturing. These include a stitched non-crimp double bias E-glass (ATL Composites, Australia), and a 3D woven glass known as Parabeam™ Para 12 mm (ATL Composites, Australia). The stacking sequence for the E-Glass composites was 8 layers at total thickness of 2.97 mm and 2 layers for 2.98 mm for Parabeam 3D-Glass composite. The composite specimens were prepared using a vacuum assisted resin infusion process. Each of the fibre reinforcements was cut and assembled in as close to as quasi-isotropic

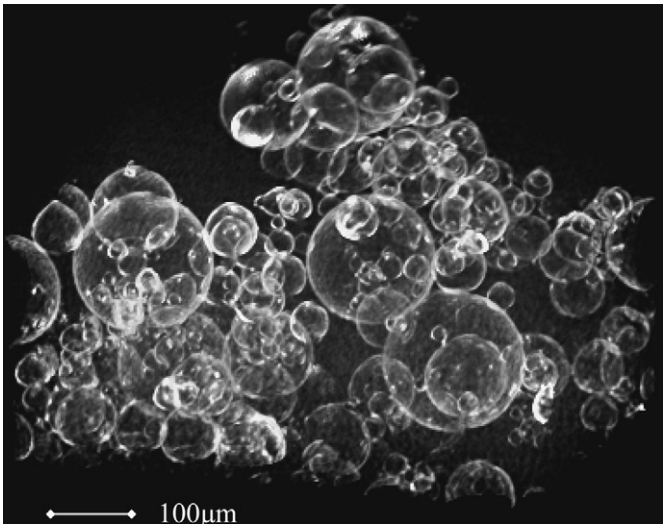

Fig. 1. Image of microsphere glass used to make polymer composite sample. The sphere size varied from 5 to 200 μm.

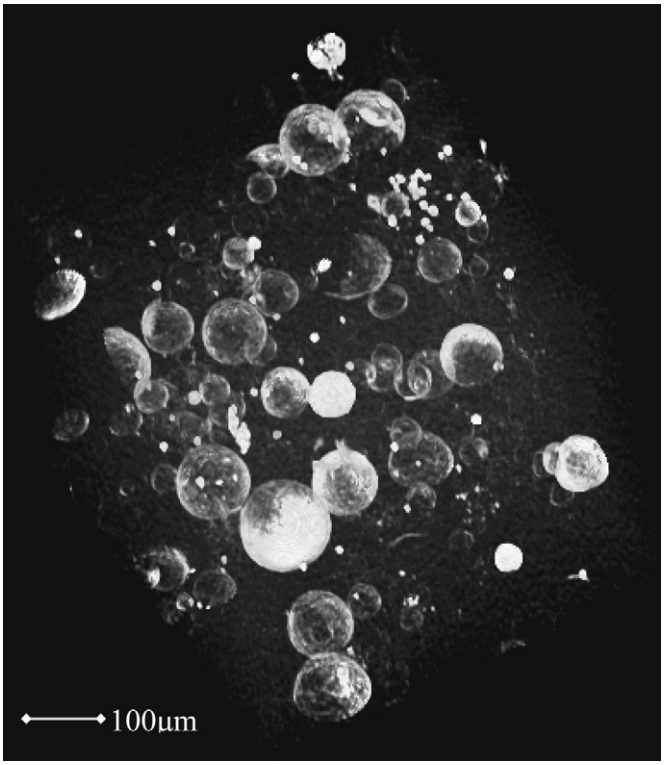

Fig. 2. Image of microlight filler used to make polymer composite sample.

lay-up as possible depending on the number of layers used in each laminate to maintain a similar cured composite thickness for each.

The Kinetix epoxy resin system was mixed at a ratio of 4 parts resin to 1 part hardener. The resin was then degassed at full vacuum for 15 min prior to infusion. The reinforcement was placed on an aluminium mould plate where K&H surface technologies SRC722 semi permanent release agent had been applied. Peel ply B and Greenflow 75 infusion medium were placed on top of the reinforcement and then vacuum bagged with Wrightlon 7400 bagging film and associated infusion hardware. The infusion took place at room temperature and was allowed to cure overnight before being debagged and trimmed. All composites were post-cured in an oven for 4 h at 100 °C.

2.2. Thermal treatment

Post-cured polymer composites of glass and microlight microspheres samples and 3D-Glass were subjected to thermal stress as follows: samples were heated in an oven to 200 °C at 5 ± 1 °C/min and kept at 200 °C for 30 h, then the samples were cooled to room temperature (22 °C) at 5 ± 1 °C/min. Another 3D-Glass sample and an E-Glass sample were heated in an oven to 240 °C at a rate of 5 ± 1 °C/min and kept at 240 °C for 30 h then cooled down to room temperature (22 °C) at cooling rate of 5 ± 1 °C/min. Two different sets of samples were produced to be used for each of the tomography and OCT tests.

2.3. X-ray microcomputed tomography instrument

X-ray microcomputed tomography imaging enables the non-destructive observation of the three-dimensional inner structure of an object by making use of the different absorption of X-rays for different materials. The tomography experiment has been performed using an *Xradia MicroXCT* instrument (Xradia, Inc., USA). In the tomography experiment, a sample is placed in the X-ray beam and rotated in an angular range between −90° and +90°. The basic principle of tomographic set-up is reported elsewhere [27]. The X-ray source is a conventional microfocus X-ray tube that uses a tungsten target. The tube voltage was 100 kV and 10 W. Source to sample distance was set to 60 mm and the sample to the detector distance is 60 mm for a geometrical magnification of 2×. Images were acquired by a scintillation/CCD composite camera coupled with 4× objective lens, giving a total magnification of 8×. A set of 721 absorption images were taken for sampling this range of rotation angles. Each projection image was acquired in 50 s. Each intensity image was corrected for the dark current image and for non-uniform illumination in the imaging system, by taking a reference image of the beam without sample. Using reconstruction algorithms, a 3D view of the sample can be computed, allowing the interior of material to be investigated non-destructively. The 3D result has a voxel size of $(3.3\ \mu m)^3$ with the field of view of $(3.15\ mm)^3$. The total reconstructed volume contains 1024 × 1024 × 1024 voxels.

2.4. Optical coherence tomography

For the investigations on the reinforced epoxy resin composite samples, two different laboratory SD-OCT set-ups have been used, one operating at a centre wavelength of 840 nm exhibiting a depth resolution of 4 μm in typical polymer materials (with refractive indices of ~1.5), the second one working with light centred around 1550 nm and with 12 μm depth resolution in polymer materials. The exact characteristics of these OCT systems can be found in reference [28]. In addition, we have used an OCT system with UHR-imaging capabilities (depth resolution < 2 μm) operating at a centre wavelength of 800 nm. This set-up additionally provides the possibility to directly acquire so-called en-face scans, i.e. areal scans located at a determined depth below the surface (image plane perpendicular to impinging light beam). The details on this en-face scanning UHR-OCT set-up can be found in reference [29]. Finally, it is worth mentioning that the samples do not have to be cut in order to obtain high resolution (like e.g. necessary for XμCT) since the OCT measurements take place in reflection geometry and the obtainable resolution is only depending on the characteristics of the OCT set-up (spot size and spectral width of light source) and not on the sample size. Consequently, extended samples and large areas can easily be investigated with high resolution, however, only up to a depth of 0.5–2 mm may be probed depending on the imaging wavelength and the scattering characteristics of the sample [26], making OCT highly suitable and convenient for the thorough structural characterisation of the surface and near-surface region.

3. Results and discussion

Initially, all the thermally treated polymer composites were tested for XμCT using the same volume of $(3.15\ mm)^3$ and same operating conditions. The tomographically examined volumes for the different composites were selected to be in the centre location. However, the volume location may have shifted slightly between the untreated and the treated samples of same composites due to the slight change in dimension as a result of the thermal treatment. The untreated samples of each composite were also tested for comparison. Crack volume calculation is carried out for the treated epoxy resin composites after heat treatment. Automatic segmentation to differentiate between the cracks and any other voids in the sample was not possible for the syntactic foam samples because of the similarity in X-ray absorption levels among the cracks, the void inside the hollow glass and the air bubbles. Hence, manual segmentation was used to locate the cracks and assign their volumes. No such difficulty was encountered in analysing the

3D-Glass and E-Glass composites due to the different X-ray absorption of their composite components.

The ratio between the crack volume and the total examined volume can be seen in Table 1 for the four different epoxy resin composites. Table 1 shows that at 200 °C and 30 h treatment, microlight microsphere resin composite showed higher cracks to the examined volume ratio than the glass microsphere and 3D resin composites. 3D-Glass resin composite showed insignificant volume of cracks at 200 °C indicating higher thermal stability. At 240 °C and 30 h treatment conditions, E-Glass resin composite showed lesser crack volume than the 3D-Glass resin composite. E-Glass composites showed less tendency to suffer cracks than 3D-Glass composites. 3D-Glass composites, at same treatment conditions, showed significantly fewer cracks than the glass microsphere and microlight microsphere resin composites. The above results show that fabric reinforced composites are more resistant to thermal degradation, since for this type of samples – in contrast to the particle filled ones – void formation is minimized during processing leading to a smaller probability of crack initiation.

The reconstructed image of the untreated and thermally treated (200 °C/30 h) glass microsphere composite samples are shown in Fig. 3. The untreated sample, slice image shown in Fig. 3a, has no cracks and no apparent sphere damage or enlarged air bubbles (over 200 μm). The glass microspheres are fairly distributed without a noticeable spheres agglomeration. However, patches of resin matrix without glass spheres can be seen. Fig. 3b shows a slice image from the 200 °C (30 h) treated sample. The image clearly shows big cracks with enlarged air bubbles (up to 700 μm). It is observed that cracks in the sample initiate from air bubbles that are originally trapped during the composite manufacturing process or resulted from the volatile degradation products of the resin. An example of a 3D image and a 2D slice of an air bubble in glass microsphere resin composite sample is presented in Fig. 4. Fig. 4a shows that the air bubbles with 615.2 μm diameter generated a crack that appears on its upper right side that fractured the adjacent glass sphere (white arrow). Fig. 4b shows that the gas bubble exhibits an irregular boundary but is strong enough to restrain the glass sphere from penetrating the bubble wall. The expansion of the air bubbles is believed to be the main cause for crack initiation and propagation.

Three-dimensional views of the crack network inside the treated glass microsphere composite sample for the whole tomographically examined volume can be seen in Fig. 5. The dimension of the rendered cube is $(2\ \text{mm})^3$. Fig. 5a shows the crack locations (white arrows) within the investigated sample size. Fig. 5b shows that the microsphere resin composite suffered considerable cracking (not to scale). Comparison between Fig. 5b and Table 1 shows that the cracks have a significant volume and are in different shapes and sizes and no pattern was detected on their distribution. Apart from air bubble enlargement, no other degradation factors such as interface rupture or matrix failure were detected. Comparison between the local density (X-ray absorption level) between the treated and the untreated samples shows no significant change.

The 2D slices of the untreated and thermally treated microlight resin composite are shown in Fig. 6. Fig. 6a showed a largely homogeneous distribution of microlight spheres. There were no clear resin patches and the air bubbles size did not exceed 300 μm. Fig. 6b shows the 2D reconstructed slice view of the microlight resin

Table 1
The volume ratio between the crack or void and the sample.

	μlight	μsphere	3D-Glass	E-Glass
200 °C, 30 h	1×10^{-2}	5.99×10^{-3}	2.75×10^{-5}	–
240 °C, 30 h	–	–	3.49×10^{-3}	2.55×10^{-3}

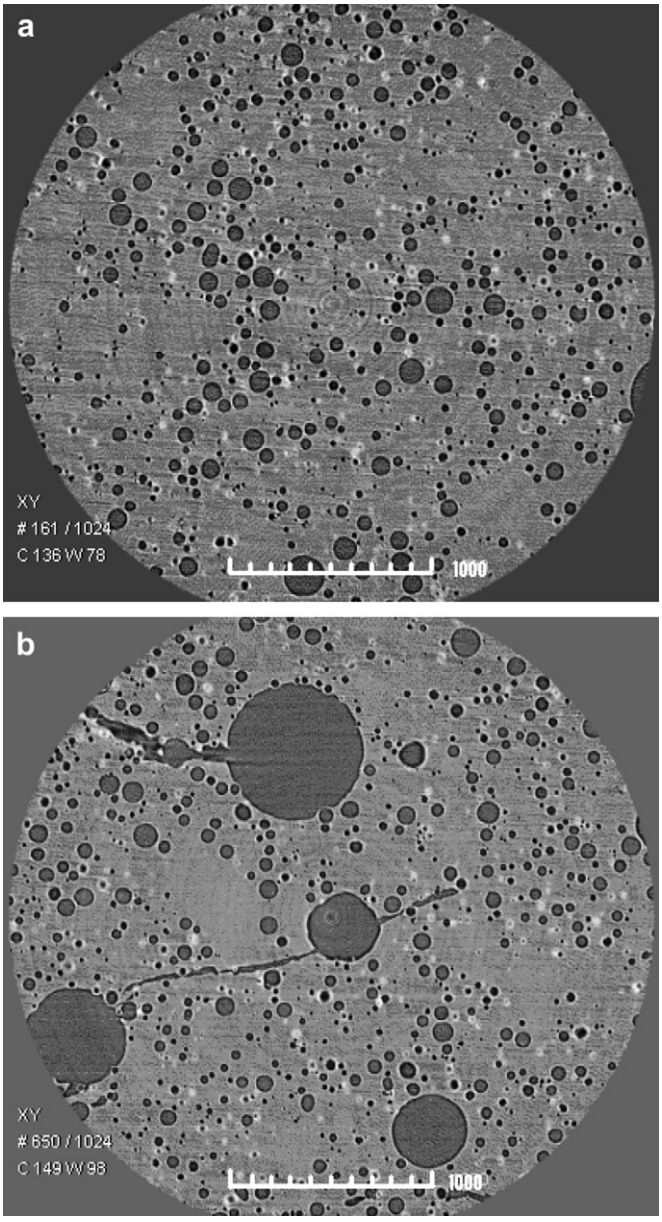

Fig. 3. Reconstructed 2D slices of (a) untreated and (b) treated (200 °C, 30 h) glass microsphere composite sample. The scale bar is in microns.

sample after the thermal treatment at 200 °C for 30 h. Similar to the glass microsphere composite sample, the cracks appear to initiate from the expanded air bubbles. However, air bubbles didn't enlarge as significantly in the microlight resin sample (<500 μm) in comparison to those of the glass microsphere composite. The cracks in the microlight composite sample are bigger and grow longer than those in the glass microsphere sample. A three-dimensional view of the cracks can be seen in Fig. 7. Fig. 7a shows the cracks = locations in the investigated sample size (white arrows). Fig. 7a also shows that the expanded air bubbles are the initiation points of the cracks. Fig. 7b shows a generated 3D image of the shapes of the cracks. The observed cracks in the microlight resin composite are mostly a network-like structure with the air bubbles as the connecting points. Fig. 8a shows a 3D image of air bubbles as an initiation point of cracks and its slice image is shown in Fig. 8b.

Fig. 9 shows the reconstructed slice images of the untreated and treated (200 °C and 240 °C at 30 h) 3D-Glass resin composite.

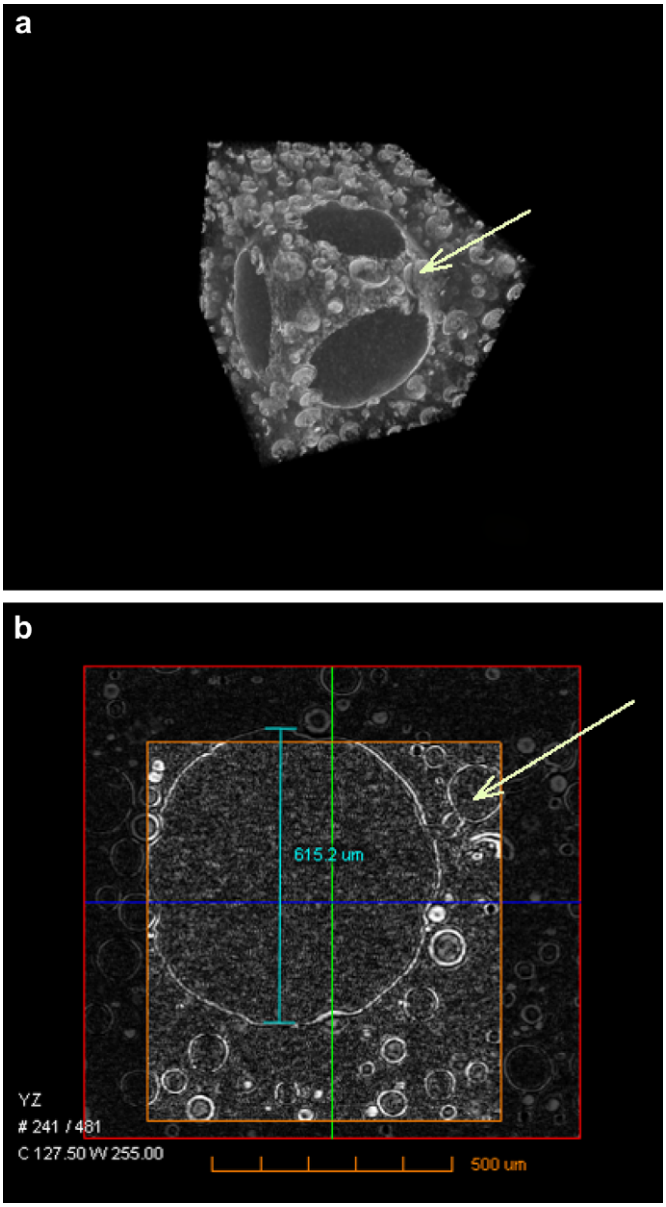

Fig. 4. (a) 3D image and (b) 2D slice image of air bubble from the treated (200 °C, 30 h) glass microsphere resin composite sample. The arrows point to the crack initiation point.

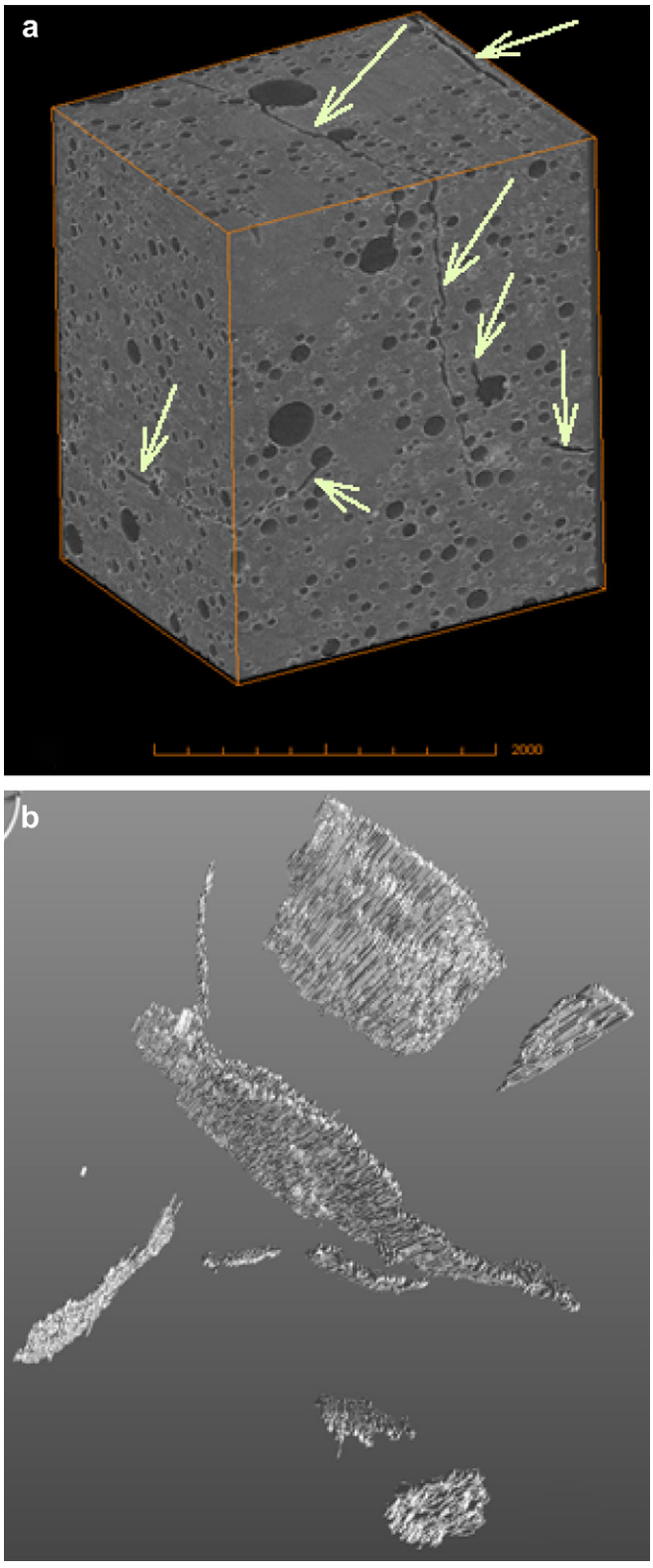

Fig. 5. (a) A three-dimensional view including crack networks inside the microsphere composite (200 °C, 30 h heated). The scale bar is in microns. (b). Distribution of the crack volume.

Fig. 9a shows the untreated resin composites with glass fabric embedded in the resin matrix without any noticeable defects. 3D-Glass resin composites suffered minor damage after treatment at 200 °C in comparison with the glass microsphere and microlight composites as shown in Fig. 9b. Small voids were generated in the resin matrix and between the fibre fabrics. The 3D-Glass fabric remained intact and the voids did not develop into crack network. A fresh sample was treated under new conditions of 240 °C for 30 h – Fig. 9c shows multiple voids and cracks resulted from the elevated temperature. Most of the voids are in the resin matrix but some also cut through the reinforcement fabric. Fig. 10 shows the treated 3D-Glass resin samples treated at 240 °C and the rendering images of the crack volume from samples treat both at 200 °C and 240 °C for 30 h. The crack/void volume is obvious inside the resin matrix and mainly grows inside it as shown in Fig. 10a. Fig. 10b shows the amount of voids that are generated in the 3D-Glass resin after the

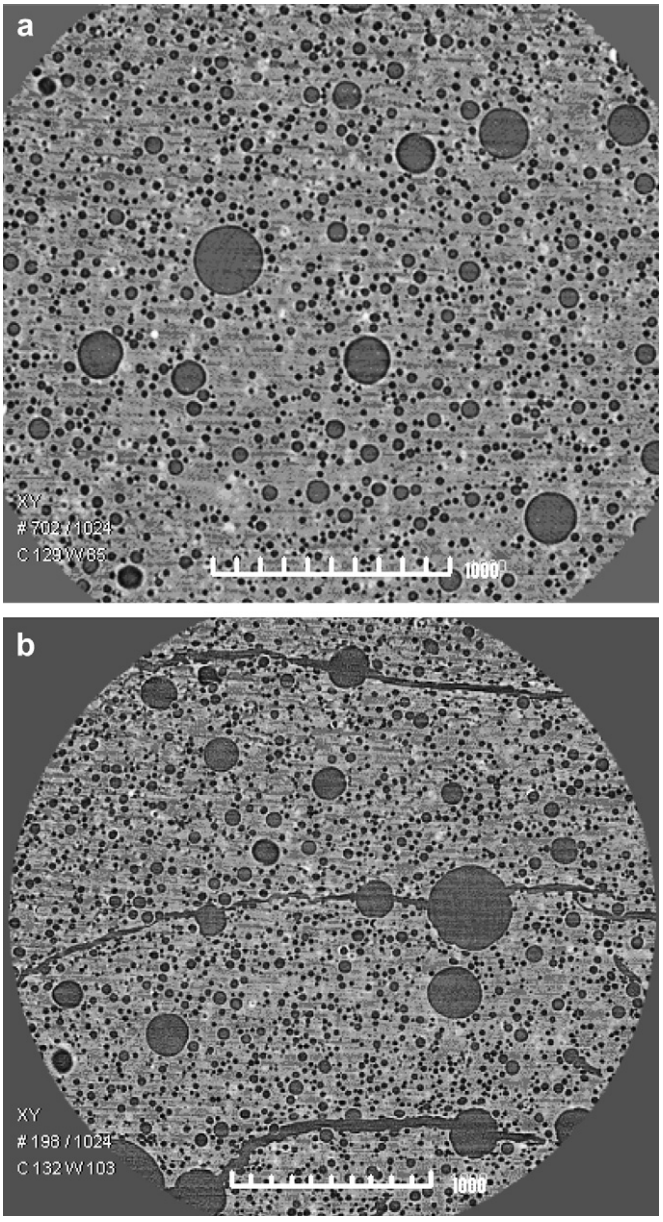

Fig. 6. Reconstructed 2D slices of (a) untreated and (b) treated (200 °C, 30 h) microlight composite sample.

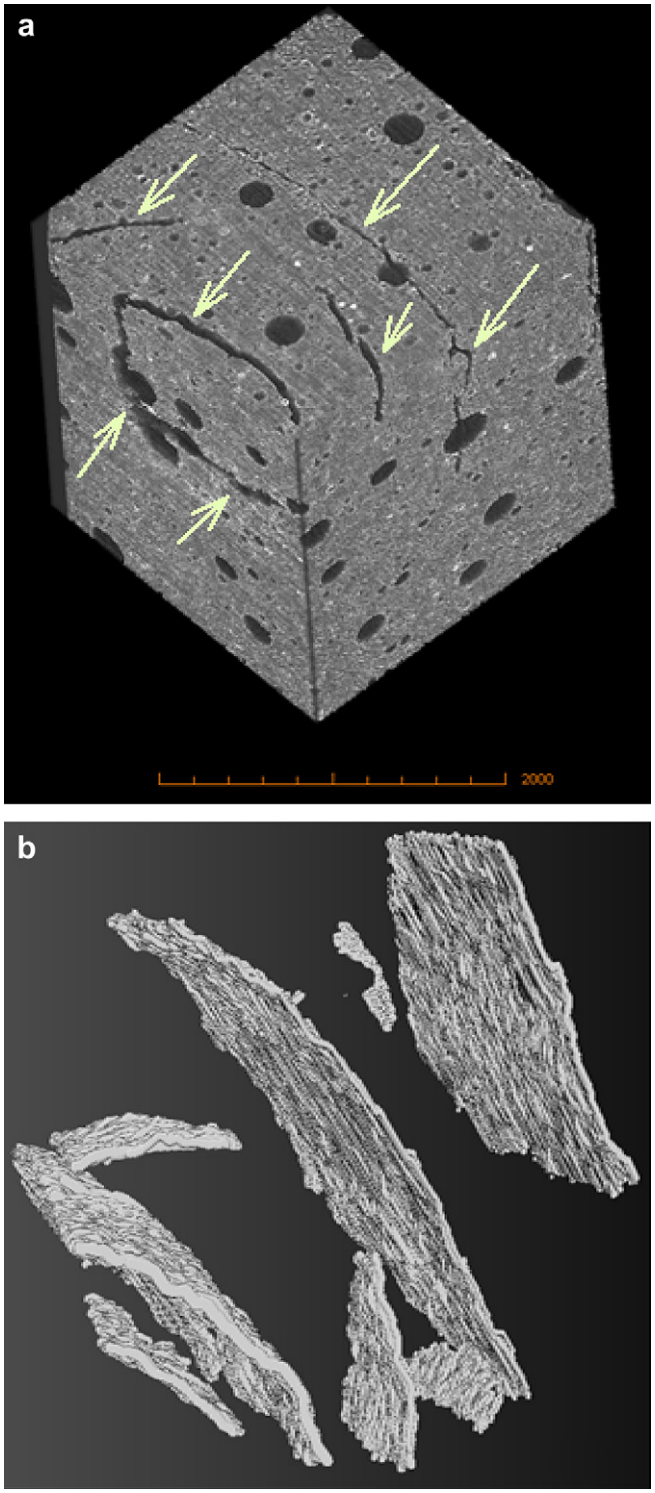

Fig. 7. (a) A three-dimensional view including crack networks inside the microlight resin composite (200 °C, 30 h heated). (b) Distribution of crack volume.

200 °C treatment while Fig. 10c shows the amount of voids after the 240 °C treatment condition. The void amount significantly increases with increasing the treatment temperature from 200 °C to 240 °C. The observed voids size ranges from large and long cracks to small voids and dents as shown in Fig. 10c with the voids/cracks volume ratio as reported in Table 1.

Fig. 11a shows the 2D slices of the treated E-Glass resin composite treated at 240 °C for 30 h. In the E-Glass resin composite voids were generated mainly in the resin matrix between the fibre fabrics, similar to the voids in the 3D-Glass composite. As explained above (see also Table 1), E-Glass composites showed the least crack volume among tested composites. Further, it is observed that the E-Glass resin composite cracks form clusters of small voids. A 3D view of the cracks formation is presented in Fig. 11b. Fig. 11c shows the rendering image of the crack volume of the E-Glass composite at 240 °C and 30 h. Since the resin matrix system and the sample thickness of the 3D-Glass and E-Glass composites are the same, the better performance of the E-Glass composites is believed to be related to the stacking sequence of the fibres. For the E-Glass composite more layers are used than for 3D-Glass, eventually providing improved geometry and decreasing the chance for cracks, generated in the resin matrix, to grow bigger.

In contrast to XμCT performed on sample regions which were cut from the interior of the untreated and treated composite

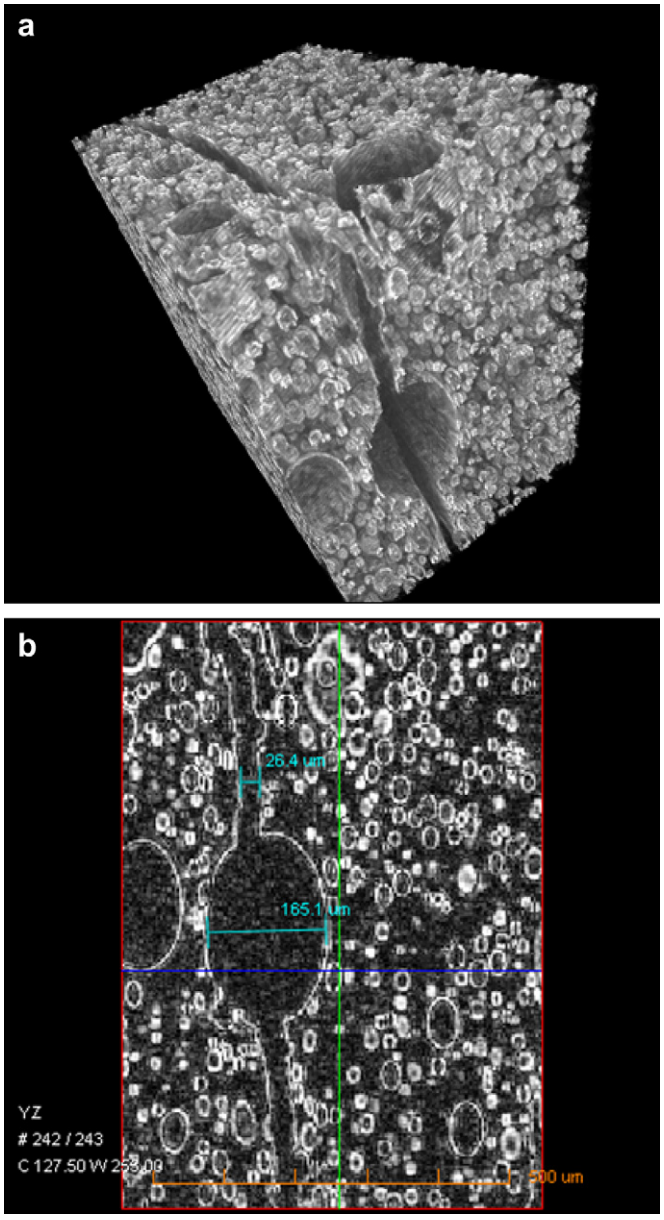

Fig. 8. 3D (a) and 2D reconstructed slice (b) of thermally treated (200 °C, 30 h) microlight composite showing a major crack.

samples, OCT was finally used in a complementary way to directly investigate structural changes of the regions close to the surface. Cross-sectional and en-face OCT images, with lateral scan ranges of up to 9 mm, were performed for the first time to elucidate effects of accelerated thermal degradation as exemplified on one of the particle-filled and on one fibre-reinforced sample in order to demonstrate the potential of this novel optical imaging technique for future routine investigations.

In Fig. 12, OCT images of the near-surface region of an untreated and treated epoxy composites with microlight microsphere filler are presented. Fig. 12a and b shows cross-sectional images taken with the 840 nm SD-OCT system. In both images point-reflections of the filler particles can be detected and it can be noticed that the distribution of the particles is not completely homogeneous: the dark irregular areas represent the matrix without particles. In contrast to the untreated sample which exhibits a smoothly curved surface (Fig. 12a), the surface of the treated sample is slightly

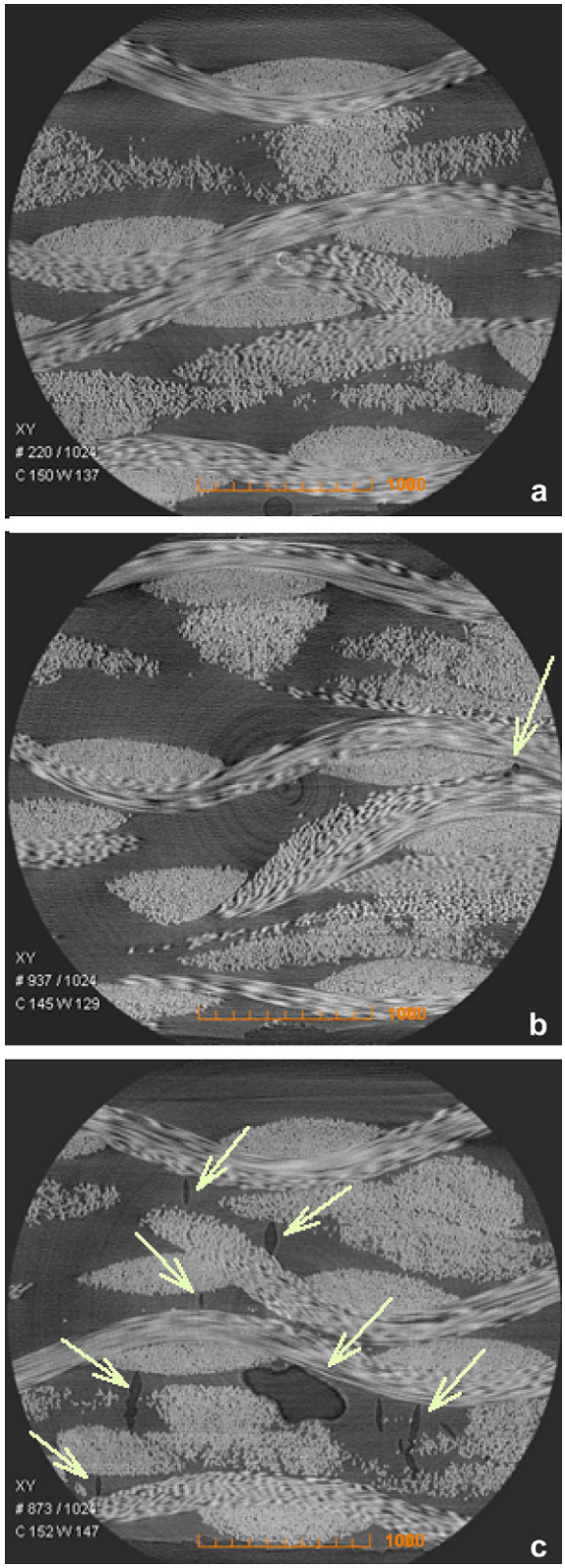

Fig. 9. Reconstructed 2D slices of 3D-Glass composite sample (a) untreated (b) treated at 200 °C, 30 h and (c) treated at 240 °C, 30 h. Arrow in (b) marks a small crack.

corrugated and sunk in the vicinity of the voids, consequently leading already open air bubbles to open even wider (Fig. 12b). The cross-sectional image in Fig. 12c was taken with the UHR-system featuring an instructive example of the resulting surface

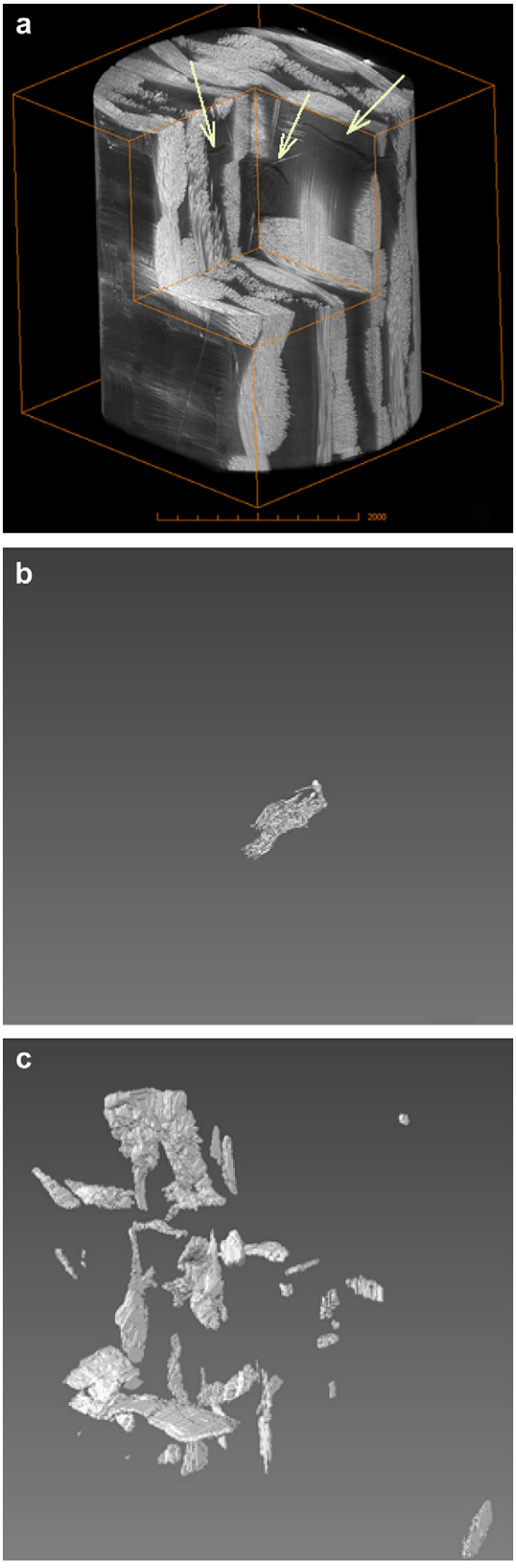

Fig. 10. A three-dimensional view of some cracks inside the 3D-Glass resin sample (a) and rendering images of 3D-Glass composites cracks at (b) 200 °C, 30 h treatment and (c) 240 °C, 30 h treatment.

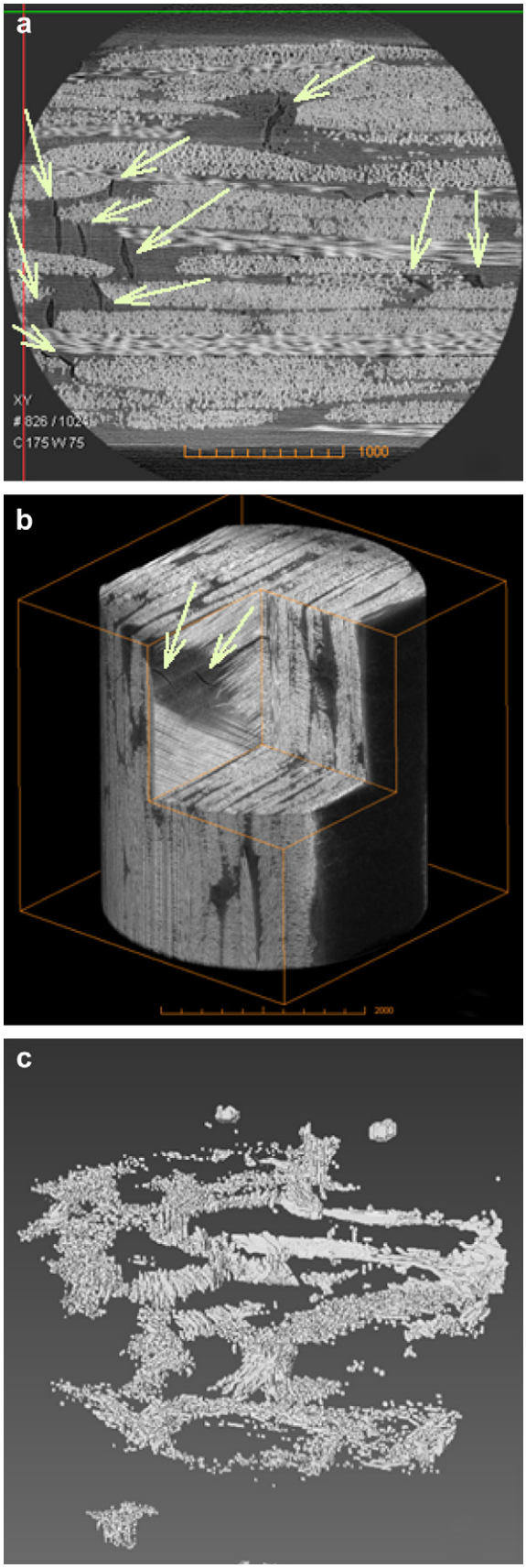

Fig. 11. Slice views of treated (240 °C, 30 h) E-Glass composite sample (a) and a three-dimensional view of some cracks inside the E-Glass resin sample (b) and its rendering volume (c).

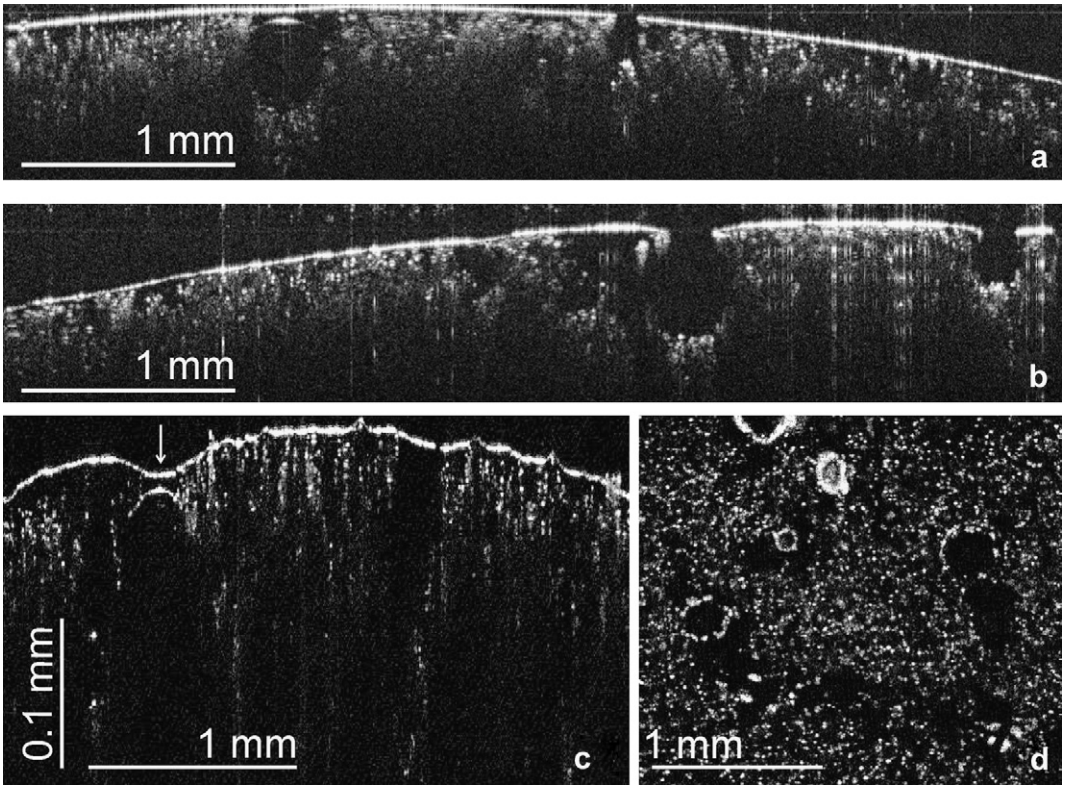

Fig. 12. OCT images taken at wavelengths around 800 nm of an untreated a) and a treated b)–d) microlight-filled sample. a) and b) are cross-sectional images with a depth resolution of 4 μm, c) is a cross-sectional image with UHR resolution (<2 μm). The arrow marks a sunken surface region located over an embedded void structure. d) represents a subsurface en-face scan taken at ~50 μm below the surface.

corrugation caused by a subsurface air bubble after treatment. From this image the minimum remaining wall thickness between void structure and surface was determined to be only 8–10 μm (indicated with arrow), with the surface sunk by an amount of even 15–20 μm as measured at this position relative to the surrounding surface area. Furthermore, it is noticed that the higher resolution of the UHR system leads to a significant improvement in resolving the individual particles, as it is also the case in the en-face scan of Fig. 12d, taken in a depth of around 50 μm below the surface. In the latter image, several air bubbles as well as regions which exhibit no particles at all (matrix only) can be distinguished.

The OCT systems operating in the 800 nm regime provide a penetration depth of 0.3–0.5 mm in the microlight microsphere filled composite, as estimated from the scans in Fig. 12. By switching to longer wavelengths a higher penetration is expected due to decreased light scattering, as it has recently been demonstrated in reference [26] on a variety of filled and unfilled polymer materials. The effect of imaging at longer wavelengths is evident in Fig. 13 where the 1550 nm SD-OCT system was used to investigate the untreated and treated microlight microsphere composite samples: the penetration depth nearly doubles in the materials, so that the locations of the subsurface air bubbles, with diameters up to 300 mm, are better discernible. Also the effect of the treatment on the state of the surface can be better judged, like void opening and surface corrugation in the vicinity of the air bubbles. However, the individual particles cannot be resolved due to the lower depth resolution of only 12 μm. Nevertheless, inhomogeneities in the overall distribution of the particles can equally be detected, as it is the case e.g. at the right end of the treated sample in Fig. 13d: over a length of nearly 1.2 mm no particles are present in the matrix up to a depth of ~80 μm (area indicated by dotted ellipse).

Finally, for comparison, the effect of thermal degradation was also studied on a fibre-reinforced composite (3D-Glass sample) in addition to the particle filled sample as presented above. The images in Fig. 14a and b represents cross-sectional scans taken at a centre wavelength of 1550 nm of an untreated and a treated sample (200 °C for 30 h), respectively. It is worth noting, that for the untreated sample, the fibre structure is nearly invisible in the OCT images. This is due to closely matching refractive indices of the fibre and matrix materials. In contrast, for the treated material, the woven structure of the fibre bundles can be better distinguished (especially visible in the right part of Fig. 14b up to an imaging depth of more than 1 mm), hinting at a modification of the materials properties which also leads to a relative change of the refractive indices. The same effect has been observed for an imaging wavelength of 800 nm (not shown).

By studying the surface topography of the untreated sample (Fig. 14a) its totally smooth appearance becomes evident (straight uninterrupted and uncorrugated bright line of the surface). In contrast, the heat treatment causes the top-most fibre bundles to affect the surface and near-surface region, visible in the areas indicate with the arrows in Fig. 14b. The top-most bundles cause surface corrugations, which show up as slightly patchy disturbances in the bright line representing the surface reflex. The UHR-OCT images in Fig. 14c and d give a detailed picture of effect of the thermal treatment to the near-surface regions. In Fig. 14c a UHR-OCT cross-section perpendicular to a top-most fibre bundle is depicted: the individual fibres of the bundles protrude in average by ~45 μm, measured relative to the average surface height located beside the bundle, an effect which is most probably due to surface shrinkage during the treatment. In case of a UHR-cross-section parallel to the fibres in the bundle (Fig. 14d), the influence of the

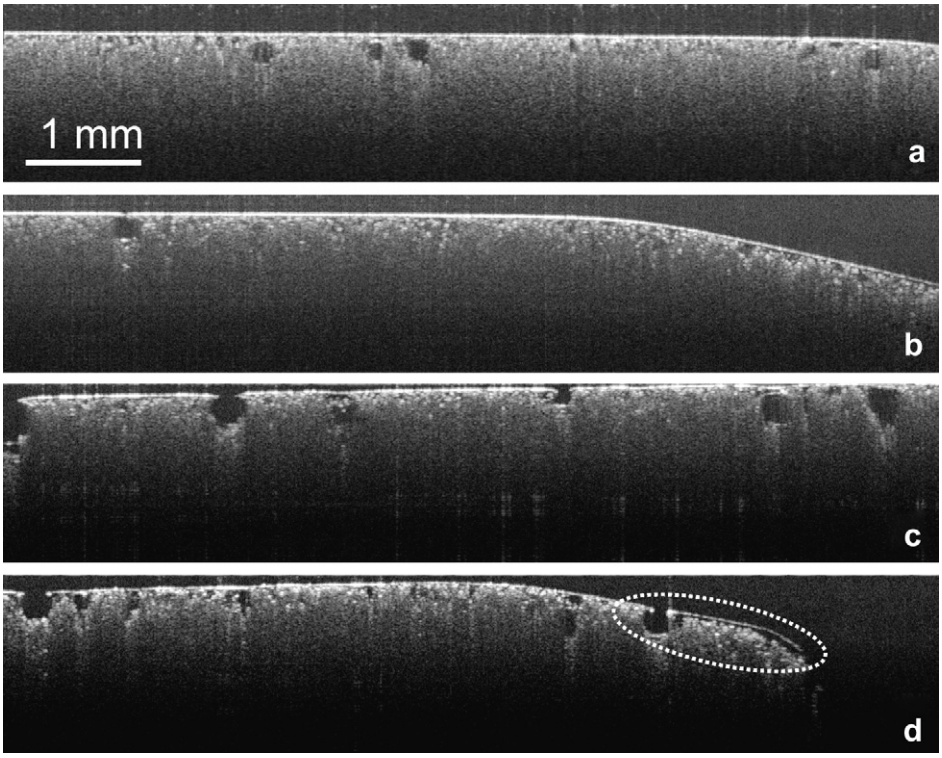

Fig. 13. Cross-sectional images taken at 1550 nm of the microlight-filled untreated a), b) and treated sample c), d). A region below the surface (adjacent to an opened bubble) which is devoid of particles is indicated in d).

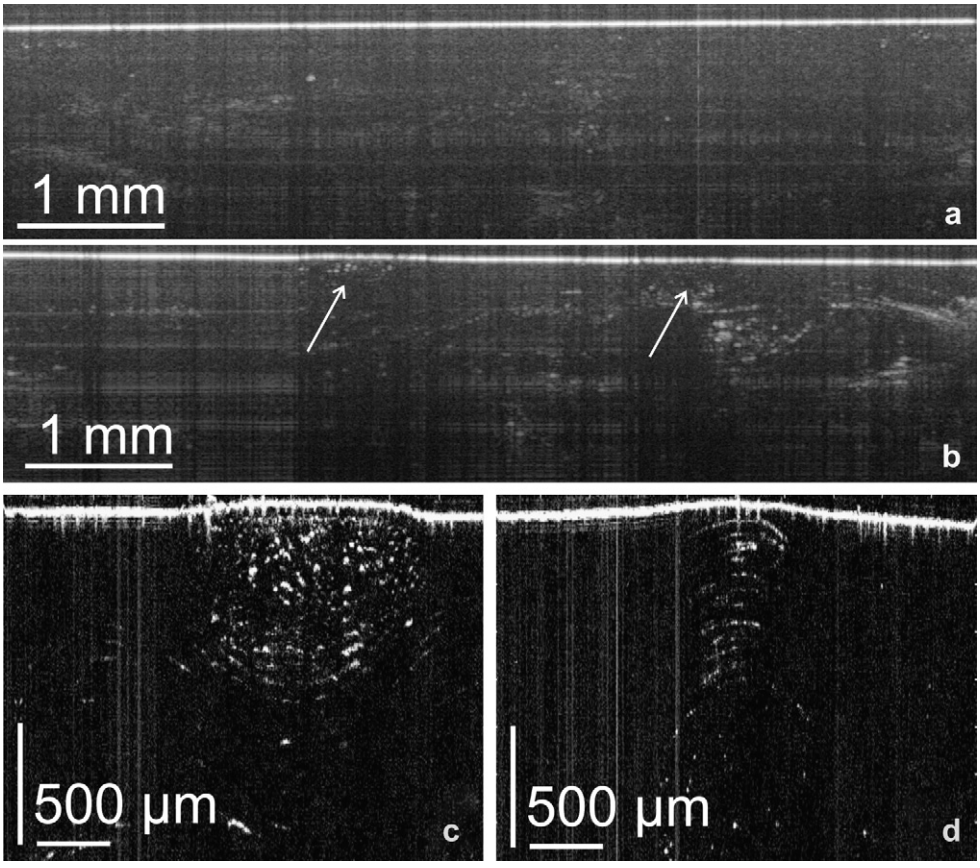

Fig. 14. Cross-sectional images taken at 1550 nm a), b) and with UHR at 800 nm c), d) from an untreated 3D-Glass sample a) and a treated one b)–d).

thermal treatment is equally visible. However, the surface roughness in this direction is smaller than perpendicular to the fibres, underlining that the geometry and direction of the fibres in the bundles is imprinted nearly one to one on the surface structure.

4. Conclusions

XμCT and OCT proved to compliment each other in examining the internal and (near-)surface structure of different epoxy resin composites subjected to accelerated thermal treatment. For XμCT, the calculation of cracks volume as a ratio to the total volume of the examined sample is a useful approach to quantitatively evaluate epoxy resin composite damage as a result of accelerated degradation conditions. XμCT images and calculations showed that E-Glass composites generated the least amount of voids/cracks as a result of the accelerated degradation conditions in comparison with the 3D-Glass, glass microsphere and microlight microsphere epoxy resin composites. It is also revealed that most of the generated cracks in the glass microsphere and microlight microsphere composites are due to the expansion of air bubbles that originally present in the composite. Cracks in the E-Glass and 3D-Glass composites generated originally in the resin matrix and propagate into the fabric filler. The strength and geometry of the fabric filler ultimately is the decisive factor in thermal resistance of the examined epoxy resins.

In a complementary way, it was demonstrated for the first time that OCT is a promising novel method to study the effect of thermal degradation on the surface and near-surface regions of particle and fibre-reinforced composites. It was shown that OCT is capable of imaging filler particles and inhomogeneities in their distribution. For comparison, cross-sectional images have been taken at different wavelengths to estimate the obtainable penetration depth, which is best with about 1 mm for the studied samples at an imaging wavelength of 1550 nm. On the other hand, UHR-OCT at 800 nm was proven to best resolve the individual particles and to deliver detailed information on the effect of the thermal treatment, like void opening and increased surface corrugation in the vicinity of air bubbles. For the fibre-reinforced samples it could be deduced that the treatment causes a relative change in the refractive index of the materials (between fibres and matrix) and leads to a distinct protrusion of the top-most fibre bundles out of the surface.

Acknowledgements

The first author would like to thank Mr. Ashley Denmead for manufacturing the E-Glass and 3D-Glass composites. The European authors thank the Austrian Science Fund FWF (project P19751-N20), the European Regional Development Fund (EFRE) and the federal state Upper Austria for financial support as well as C.K. Hitzenberger and his group (Medical University of Vienna) for help in the realization of the OCT set-ups.

References

[1] Koopman M, Chawla KK, Carlisle KB, Gladysz GM. Microstructural failure modes in three-phase glass syntactic foams. J Mater Sci 2006;41:4009–14.
[2] Sauvant-Moynot V, Gimenes N, Sautereas H. Hydrolytic ageing of syntactic foams for thermal insulation in deep water: degradation mechanisms and water uptake model. J Mater Sci 2006;41:4047–54.
[3] Seamark MJ. Use of syntactic foam for subsea buoyancy. Cell Polym 1991; 10(4):308–12.
[4] Peters ST. Handbook of composites. Chapman and Hall; 1998.
[5] Kelly V. Carbon fibre, manufacture and application. Elsevier; 2004.
[6] Aird F. Fiberglass and composite materials. Berkley Publishing Company; 1996.
[7] Pang JW, Bond IP. A hollow fibre reinforced polymer composite encompassing self-healing and enhanced damage visibility. Compos Sci Technol 2005;65:1791–9.
[8] Dry C. Procedures developed for self-repair of polymer matrix composite materials. Compos Struct 1996;35:263–9.
[9] Aymerich F, Priolo P. Characterization of fracture modes in stitched and unstitched cross-ply laminates subjected to low-velocity impact and compression after impact loading. Int J Impact Eng 2008;35(7):591–608.
[10] Niezgoda T, Barnat W. Analysis of protective structures made of various composite materials subjected to impact. Mater Sci Eng 2008;483-484:705–7.
[11] Greenhalgh E, Bishop SM, Bray D, Hughes D, Lahiff S, Millson B. Characterisation of impact damage in skin-stringer composite structures. Compos Struct 1996;36:187–207.
[12] Ray BC. Temperature effect during humid ageing on interfaces of glass and carbon fibers reinforced epoxy composites. J Colloid Interf Sci 2006;298:111–7.
[13] Hong S. The thermal-oxidative degradation of an epoxy adhesive on metal substrates: XPS and RAIR analyses. Polym Degrad Stabil 1995;48:211–8.
[14] Rose N, Le Bras M, Delobel R, Costes B, Henry Y. Thermal oxidative degradation of an epoxy resin. Polym Degrad Stabil 1993;42:307–16.
[15] Chaturvedi M, Shen YL. Thermal expansion of particle-filled plastic encapsulant: a micromechanical characterization. Acta Mater 1998;46(12):4287–302.
[16] Lafarie-Frenot MC, Rouquiéa S, Hoa NQ, Bellenger V. Comparison of damage development in C/epoxy laminates during isothermal ageing or thermal cycling. Compos Part-A Appl S 2006;37:662–71.
[17] Decelle J, Huet N, Bellenger V. Oxidation induced shrinkage for thermally aged epoxy networks. Polym Degrad Stabil 2003;81:239–48.
[18] Olivier L, Baudet C, Bertheau D, Grandidier JC, Lafarie-Frenot MC. Development of experimental, theoretical and numerical tools for studying thermo-oxidation of CFRP composites. Compos Part-A Appl S 2008; doi:10.1016/j.compositesa.2008.04.005.
[19] Hancox NL. Thermal effects on polymer matrix composites: part 1. Thermal cycling. Mater Des 1998;19:85–91.
[20] Beier U, Fischer F, Sandler J, Altstädt V, Weimer C, Buchs W. Mechanical performance of carbon fibre-reinforced composites based on stitched preforms. Compos Part-A Appl S 2007;38:1655–63.
[21] Awaja F, Arhatari BD. X-ray micro computed tomography investigation of accelerated thermal degradation of epoxy resin/glass microsphere syntactic foam. Composites: Part A 2009; doi:10.1016/j.compositesa.2009.05.014.
[22] Schilling PJ, Karedla BR, Tatiparthi AK, Verges MA, Herrington PD. X-ray computed microtomography of internal damage in fiber reinforced polymer matrix composites. Compos Sci Technol 2005;65:2071–8.
[23] Huang D, Swanson EA, Lin CP, Schuman JS, Stinson WG, Chang W, et al. Optical coherence tomography. Science 1991;254:1178–81.
[24] Bouma BE, Tearney GJ. Handbook of optical coherence tomography. New York: Dekker; 2002.
[25] Leitgeb R, Hitzenberger CK, Fercher A. Performance of Fourier domain vs. time domain optical coherence tomography. Opt Express 2003;11:889–94.
[26] Stifter D. Beyond biomedicine: a review of alternative applications and developments for optical coherence tomography. Appl Phys B 2007;88:337–57.
[27] Kak AC, Slaney M. Principles of computerized tomographic imaging. New York: IEEE Press; 1988.
[28] Stifter D, Wiesauer K, Wurm M, Schlotthauer E, Kastner J, Pircher M, et al. Investigation of polymer and polymer/fibre composite materials with optical coherence tomography. Meas Sci Technol 2008;19:74011–8.
[29] Wiesauer K, Pircher M, Götzinger E, Bauer S, Engelke R, Ahrens G, et al. En-face scanning optical coherence tomography with ultra-high resolution for material investigation. Opt Express 2005;13:1015–24.